# Stabilization of high-spin Mn ions in tetra-pyrrolic configuration on copper

Silvia Carlotto [a,b], Javier D. Fuhr [c], Albano Cossaro [d,e], Alberto Verdini [e], Maurizio Casarin [a], Magalí Lingenfelder [f], Julio E. Gayone [g], Luca Floreano [e,*], Hugo Ascolani [g,*]

[a] Department of Chemical Sciences, University of Padova, Via F. Marzolo 1, 35131 Padova, Italy
[b] CNR-ICMATE, Via F. Marzolo 1, 35131 Padova, Italy
[c] Instituto de Física del Sur, UNS-CONICET, Av. Alem 1253, Bahía Blanca, Argentina
[d] Department of Chemistry and Pharmaceutical Science, University of Trieste, I-34127 Trieste, Italy
[e] CNR-IOM, Laboratorio TASC, Basovizza SS14 Km. 163.5, I-34149 Trieste, Italy
[f] Max Planck-EPFL Laboratory for Molecular Nanoscience, E´cole Polytechnique F´ed´erale de Lausanne, Switzerland
[g] Centro At´omico Bariloche, CNEA, and CONICET, Av. E. Bustillo 9500, R8402AGP Bariloche, Argentina

ARTICLE INFO

*Keywords:*
Mn-TCNQ network
Sn-Cu alloying
High spin Mn
ROCIS method
NEXAFS

ABSTRACT

By means of Mn-Cu transmetalation, we incorporated Mn atoms in an array of TCNQ (7,7,8,8-tetracyanoquinodimethane) grown on Cu(100), forming a long range ordered and commensurate metal–organic coordination network (MOCN). Preliminary Sn alloying of the Cu(100) surface allowed us to control the degree of substrate reactivity, thus preventing the chemical interaction of the Mn-TCNQ MOCN with the substrate. $Mn^{2+}$ ions are stabilized in an artificial tetra-pyrrolic coordination, which mimics the macrocyle configuration of Mn-phthalocyanines/porphyrins. X-ray absorption spectroscopy at the Mn $L_{2,3}$-edge indicates that the Mn ions are in a high-spin state (S = 5/2), in agreement with DFT + U calculations which also shows that the electronic structure of this Mn-TCNQ MOCN is very similar to that of the corresponding unsupported MOCN.

Low dimensional structures based on arrays of molecular magnets have a high potential for their integration in magnetic recording, spintronic and sensing devices thanks to the possibility of tuning the magnetic and chemical properties of the individual subunits by suitable choice of the metallic centre. A considerable effort is dedicated to grow and investigate two-dimensional (2D) metal–organic coordination networks (MOCNs) confined on surfaces, where the periodically arranged metal centers are magnetically coupled by the organic ligands.

A consolidated strategy to produce modular 2D-MOCNs was developed, which consists in the co-deposition of the building blocks, i.e. atoms and organic molecules, directly on crystalline surfaces of coinage metals [1,2]. This method constitutes a powerful tool for the engineering of surface-supported 2D metal–organic materials with magnetic order [3–8]. A prototypical case of 2D-MOCN with anti-ferromagnetic order is the rectangular Mn-TCNQ network grown on Au(111) by Faraggi et al. [5,7,8]. The experimental observations are in agreement with the results of DFT (density functional theory) calculations for the corresponding unsupported rectangular Mn-TCNQ (7,7,8,8-tetracyanoquinodimethane) network [8,9] and other similar structures [10], which predict a high-spin (HS) configuration (S = 5/2) for $Mn^{2+}$ ions coordinated to nitrogen atoms in a tetraplanar geometry.

So far, the study of magnetic properties of MOCNs has been limited to noble metal substrates, such as Au and Ag, whereas the direct or indirect coupling to a ferromagnetic substrate would be much useful to study the dynamics of magnetism and magnetization (reversal, reorientation). The intercalation of non-magnetic layers between magnetic films (either organic or inorganic) is a common practice in the engineering of spin valve structures. In this regard, copper is ideally suited to grow buffer layers on the most relevant magnetic metals thanks to its optimal structural coupling (pseudomorphism) to Co, Fe, Ni crystals and films [11–17], thus preserving surface flatness and, eventually, long range order, which are prerequisites in a bottom-up self-assembly strategy. As a consequence, the possibility of producing magnetic MOCN, as well as molecular films, on copper would be highly desirable. On the other hand, the relatively large reactivity of Cu strongly affects the self-assembly and electronic structure of organic molecules [10], thus limiting the on-surface synthesis of a MOCN. In addition, even the metal centres of chemically robust organo-metallic complexes, such as metal-porphyrins and derivatives, have been demonstrated to strongly interact with Cu substrates, yielding dramatic changes of the metal electronic

structure [18], or metal replacement by substrate Cu atoms (transmetalation) [19–22].

These limitations can be overcome by tailoring the surface alloying of Cu(100) with Sn atoms in order to tune the degree of reactivity of the substrate [23–26]. In particular, the $(\sqrt{3} \times 2\sqrt{2})R45^\circ$ reconstruction of the Sn/Cu(100) interface (from hereafter the $\sqrt{3}\ 2$), consisting of 0.5 ML of Sn atoms embedded in the top surface layer of the Cu(100) crystal, is a robust substrate for self-assembled supramolecular structures. We have recently reported the molecular self-organization of Mn and TCNQ into a rectangular MOCN onto the $\sqrt{3}\ 2$, whose geometry is very similar to that observed on Au(111), but with the additional advantage of displaying long range order [27]. This organo-metallic compound, with a 1 : 1 stoichiometry ratio, displays Mn atoms in a quasi-planar tetra coordination to nitrile ligands, closely resembling that of Mn-phthalocyanine/porphyrin.

In order to study the potential relevance for magnetism of this MOCN, we studied the near-edge X-ray absorption fine structure (NEXAFS) at the Mn $L_{2,3}$-edge of the Mn-TCNQ/$\sqrt{3}\ 2$ interface. The X-ray absorption spectroscopy (XAS) technique is unanimously recognized as a powerful tool able for probing the molecular unoccupied electronic structure through the excitation of the core electrons of the absorbing species to the low-lying empty molecular orbitals (MOs). One of the most relevant XAS peculiarities is the local character of core excitations, which makes K- and L-edge spectra sensitive to both the electronic structure and the local surroundings of the target species. Transition metal (TM) $L_{2,3}$-edges features are determined by electronic states generated by the electric-dipole allowed $2p \rightarrow 3d$ excitations, and even though a huge amount of chemical information may be mined from them, a demanding theoretical analysis is needed to this end. As a matter of fact, besides ligand-field and TM-ligand covalency effects, the spin–orbit coupling (SOC) among the possible many final-state multiplets should be considered [28–31].

Despite the periodicity of the surface-supported Mn-TCNQ 2D pattern, the localized character of the core excitations and, most importantly, the negligible adsorbate/substrate interactions allowed us to model the XAS resonances by means of a small cluster, whose coordinates were obtained by periodic calculations. Notably, the model reproduces the main features of the experimental Mn $L_{2,3}$-edge remarkably well and clearly favours $Mn^{2+}$ ions with a high-spin (HS) state (5 unpaired electrons).

## 1. Methods

The scanning tunneling microscopy (STM) image shown in Fig. 1 was obtained at room temperature using an ultrahigh vacuum system from Omicron Nanotechnology. See reference [27] for details. We performed the XAS experiments at the ALOISA beamline of the Elettra Synchrotron (Trieste) [32]. The MOCN films were prepared in situ, following the protocols described in Ref. [27]. In particular, the TCNQ molecules were first sublimated on the $\sqrt{3}\ 2$ substrate kept at 150 °C, followed by cooling to enable the formation of ordered networks of TCNQ molecules coordinated to Cu adatoms [33]. Subsequently, Mn atoms were deposited on the prepared Cu-TCNQ/$\sqrt{3}\ 2$ surface kept at a fixed temperature between 80 °C and 150 °C. In this temperature range, no significant differences were observed neither in the measured core-level photoemission spectra (see reference [27]) nor in the NEXAFS ones.

The XAS measurements were performed with a linearly polarized photon beam, while keeping the surface at constant grazing angle of 6° and rotating the sample around the photon beam axis in order to change the surface orientation from transverse-Magnetic (TM, or nearly *p*-polarization) to transverse-Electric (TE, or *s*-polarization) polarization [34]. We measured the NEXAFS resonances in partial electron yield by means of a channeltron, which is equipped with a grid polarized to −590 V in order to reject low energy secondary electrons. The absolute photon energy calibration was performed by measuring a reference photoemission spectrum at the beginning of each NEXAFS scan.

The structure of the MOCN complex on the $\sqrt{3}\ 2$ substrate was formerly computed by DFT + U theory using Quantum ESPRESSO [35]. The calculation details can be found in our previous study of the TCNQ assembly on the Sn/Cu alloy [27]. The spin-resolved projected density of states (PDOS) on the MOCN components is shown in the SI file. The DFT structural details of the Mn-TCNQ complex have been used to derive a small cluster for the simulations of the Mn $L_{2,3}$ NEXAFS resonances. The modeling of the $L_{2,3}$-edge spectra has been carried out by exploiting the ORCA program package [36]. We adopted the meta-hybrid M06 functional [37] in connection with the def2-TZVP(-f) basis set [38], which we demonstrated to be the most performing among exchan- ge–correlation (XC) functionals for reproducing the $L_{2,3}$-edge spectra of Mn complexes [30,39,40]. We evaluated the Mn $L_{2,3}$ excitation energies (EEs), transition dipole moments and their intensities by employing the DFT/ROCIS method [41], which includes SOC in a molecular Rus- sell–Saunders fashion. The combined use of DFT and CI needs three semi-empirical parameters (c1 = 0.18, c2 = 0.20, and c3 = 0.40) [42]. Throughout the numerical experiments, we adopted the zeroth order regular approximation (ZORA) to treat the scalar relativistic effects [43], and we used the resolution of the identity approximation [44] with the def-TZVP/J basis set. The simulated spectra have been shifted to superimpose the highest intensity feature of the experimental $L_3$-edge.

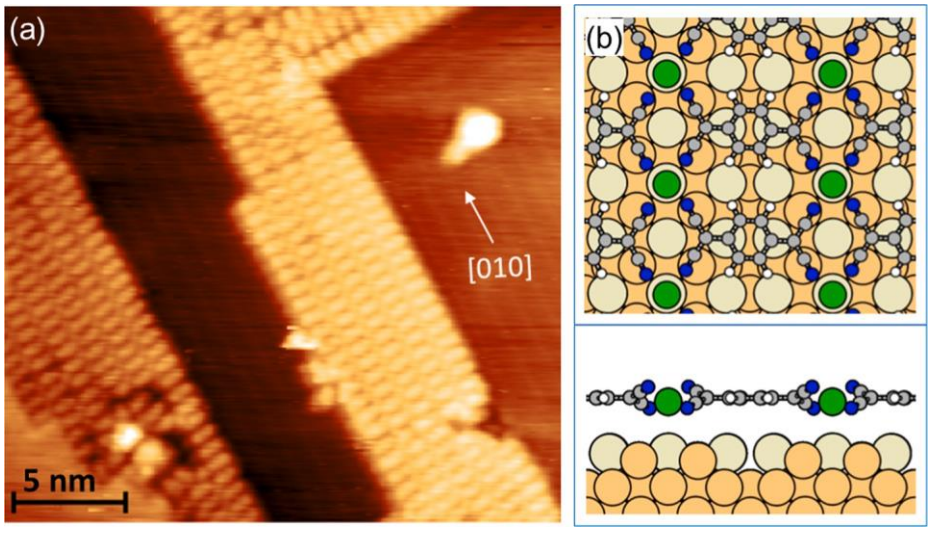


**Fig. 1.** Mn-TCNQ metal–organic coordination network formed on the $\sqrt{3}\ 2$ reconstruction. (a) STM image of the surface obtained after deposition of Mn on a TCNQ/$\sqrt{3}\ 2$ interface kept at ∼80 °C. Tunneling conditions: (+2 V/ 150 pA). (b) Top and side views (top and bottom, respectively) of the structure obtained by minimization-energy calculations [27]. Grey, white, blue and green spheres correspond to C, H, N and Mn atoms, respectively. $\sqrt{3}\ 2$ reconstruction: light-grey (orange) spheres correspond to Sn(Cu) atoms. (For interpretation of the references to colour in this figure legend, the reader is referred to the web version of this article.)

This region, differently from $L_2$ one, does not suffer of extra broadening and distortion due to the Coster-Kronig Auger decay process [45,42]. Finally, we applied a Gaussian broadening to model the $L_{2,3}$-edge NEXAFS spectra.

## 2. Results

We have previously demonstrated that deposition of TCNQ molecules on the $3\sqrt{2}$ Sn/Cu(100) reconstruction leads to the formation of several kind of MOCNs made of TCNQ molecules coordinated to native Cu adatoms [33]. When molecular deposition takes place at a surface alloy temperature of 150 °C, two coexisting ordered-phases $\beta$ and $\gamma$ are observed, where the Cu ions are coordinating 2 and 3 nitrile groups, respectively. Subsequently, the Cu adatoms are replaced by the incoming Mn atoms and, at the same time, a TCNQ rearrangement/reorientation takes place resulting in the MOCN structure formed by a 1 : 1 metal to TCNQ ratio with Mn in a nearly planar, squared, fourfold coordination to TCNQ [27]. A representative topographic STM image of the Mn-TCNQ MOCN appearance is shown in Fig. 1(a). The corresponding unit cell derived from LEED patterns displays a $\begin{pmatrix} \sqrt{3} & 2 \\ 2 & \sqrt{2} \end{pmatrix} R45$, which corresponds to a nominal molecular coverage of 1/12 ML (1 ML defined by the Cu atomic density in the (100) plane).

In contrast with the equivalent Mn-TCNQ structure formed on the Au (111) surface, the present MOCN is commensurate with the substrate and forms large and long range ordered domains [27]. Most importantly, this experimental evidence allows us to model the interface by means of a precise atomic model in the framework of periodic DFT calculations. Fig. 1(b) shows top and side views of the relaxed atomic structure derived from DFT calculations including the $3\sqrt{2}$ substrate [27]. The Mn ions are located very close to the plane of the molecular backbone (0.25 Åbelow the C-rings, which implies a large Mn-substrate distance (∼ 3.4 Åfrom the Sn layer). Remarkably, the same calculation framework for a free-standing Mn-TCNQ unit cell yields very similar structural and electronic configurations to the supported film. In particular, not only the squared molecular geometry, but also the Mn to nitrogen atoms distance is preserved (∼ 2.1 Å), as well as the characteristic twisting of the CN groups with respect to the C-ring plane, where two N atoms fall below and two above the aromatic plane (see Figure S1 for the DFT calculated structure of the unsupported layer) [27].

As expected, the projected density of states (PDOS), obtained by DFT + U calculations, of both Mn and TCNQ shows that the differences between the supported and free-standing films are very small for the occupied electronic states, meaning that the substrate does not affect significantly the Mn-ligand hybridization (see Fig. S2 of SI file). The comparison of the *d*-decomposed PDOS on the Mn atoms (see Figure S3 of SI) shows that also the ligand-field is unchanged by the substrate.

In order to measure the unoccupied electronic states, we measured X-ray absorption spectra. Although corresponding to excited states, the NEXAFS resonances are a direct probe of the empty molecular orbitals with specific chemical sensitivity. The experimental absorption spectra at the K-edge of carbon and nitrogen, as well as at the manganese $L_{2,3}$-edge, are shown in Figs. 2 and 3, respectively. Fig. 2 compares the N and C NEXAFS resonances obtained from a Mn-TCNQ MOCN with those corresponding to the initial Cu-TCNQ MOCN. Clearly, adding Mn to the Cu-TCNQ MOCN does not induce any significant change in either of the two absorption edges. Peaks $2_a$ and $2_b$ of the nitrogen NEXAFS spectra (top panel of Fig. 2) are associated with two orthogonal $\pi^*$-orbitals of the CN group [46,47]. The nitrogen NEXAFS spectra of bulk TCNQ molecules is known to bear an additional peak at about 397–398 eV (position marked by an arrow in the top panel of Fig. 2), also associated with the ring [46,47]. In agreement with the X-ray photoelectron spectroscopy (XPS) results reported in our prior article on this system [27], we interpret the absence of this extra peak in the nitrogen K-edge adsorption spectrum as the result of charge-transfer populating the LUMO orbital. The resonances 6 and 7 of the carbon NEXAFS spectra (see

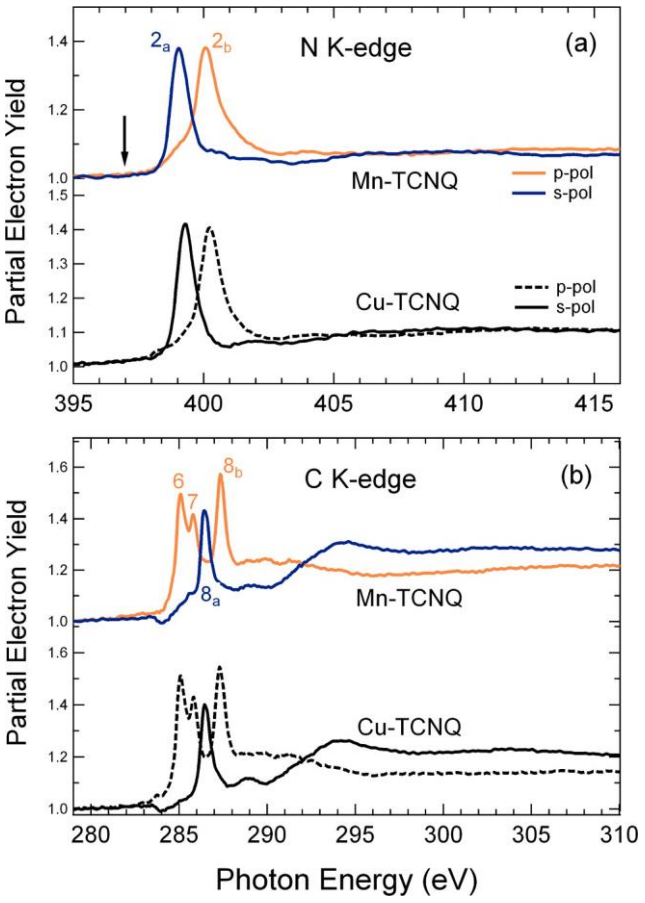


**Fig. 2.** Comparison of the experimental absorption spectra at the N and C K edges corresponding to the Mn-TCNQ/$3\sqrt{2}$ sample prepared with ∼1/10 ML of Mn with those corresponding to the Cu-TCNQ/$3\sqrt{2}$ one. The obtained Mn-TCNQ was obtained after deposition of Mn on a TCNQ/$3\sqrt{2}$ interface kept at 150 °C.

bottom panel of Fig. 2) are associated with the molecular ring, whereas resonances $8_a$ and $8_b$ stem from two orthogonal $\pi^*$-orbitals of the CN group [46,47]. The change of intensity of the resonances with the orientation of the polarization, as observed at the N and C *K*-edge, are consistent with an adsorption geometry of the TCNQ molecules closely planar and parallel to the surface.

Fig. 3 compares typical $L_{2,3}$-edge absorption spectra of the Mn-TCNQ/$3\sqrt{2}$ interface (top panel), with the one corresponding to 1/9 ML of Mn deposited on the bare $3\sqrt{2}$ substrate (bottom panel). We note that Mn/$3\sqrt{2}$ spectra display a broad and unresolved tail of both the $L_2$ and $L_3$ peaks, which is typical of a metallic state $Mn^0$. The spectra corresponding to the Mn-TCNQ network present an overall narrowing of the spectral resonances and a well-defined multiplet fine structure. The $L_3$ line is found at an excitation energy (EE) of 640.7 eV for any orientation of the polarization. Additional shoulders and satellites are clearly observed at both sides of the peak, namely at EEs of ∼ 639.9, ∼ 642,2 and ∼ 644.4 eV. On the other hand, the $L_2$ line is composed of two main resonances at EE = 651.0 eV and EE = 652.9 eV.

The multiplet structure at the Mn $L_{2,3}$-edge reflects not only the metal ionization state, but also the local spin orbit configuration [48,49]. In particular, the spin configuration of the $Mn^{2+}$ ions in a coordinative environment with four nitrogen atoms can yield different total spin values depending on the particular molecule considered. In fact, the total spin value computed for free Mn-porphyrins is S = 5/2, which corresponds to the high-spin (HS) electronic configuration that is expected for a half-filled 3d shell with strong Hund's rule coupling [50]. In

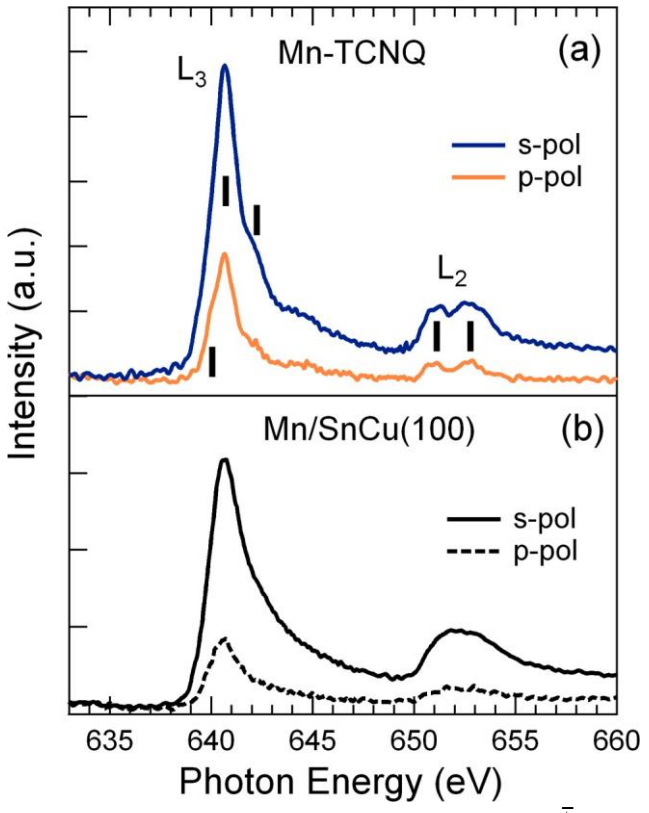


**Fig. 3.** (a) Typical $L_{2,3}$-edge absorption spectra of the Mn-TCNQ/3$\sqrt{2}$ interface prepared with 1/10 ML of Mn coverage. The vertical lines indicate the main observed structures. The obtained Mn-TCNQ was obtained after deposition of Mn on a TCNQ/3$\sqrt{2}$ interface kept at 150 °C. (b) $L_{2,3}$-edge absorption spectra corresponding to 1/9 ML of Mn atoms diluted in the bare 3$\sqrt{2}$ surface.

contrast with the latter class of molecules, the total spin found in Mn-phthalocyanines is S = 3/2 (intermediate-spin, IS) [51,52]. In this case, however, Stepanow et al. showed that the IS configuration of the Mn ions in Mn-phthalocyanines molecules adsorbed on Ag(111) can be changed to HS by reducing the crystal field through Li doping [51]. Our DFT + U calculations suggest that the $Mn^{2+}$ ions in the Mn-TCNQ monolayer are in a HS state. The corresponding magnetic moment of 5 $\mu_B$ per unit cell is predicted to be localized at the $Mn^{2+}$ ion (∼ 80%) and partly at the coordinated nitrogen atoms (see Fig. S3 of SI). We remark that, despite the close similarity of the present Mn-N bond length (2.1 Å) to that of Mn-porphyrins [50], the coincidence of the HS state is simply accidental, because of the very different structural and electronic configuration of the nitrogen ligands: embedded in a conjugated macrocycle for porphyrins, belonging to four distinct molecules for the Mn-TCNQ complex.

In order to unequivocally determine the effective ionization and spin state of the Mn ion, we simulated the NEXAFS resonances at the Mn $L_{2,3}$-edge for the two most relevant configurations, namely $Mn^{2+}$ in either intermediate or high spin state. The very weak interaction of the MOCN with the SnCu(100) surface and the localized character of the core excitations allowed us to model the Mn $L_{2,3}$ spectra by means of a small cluster, whose relevant coordinates were derived from the relaxed DFT model of the adsorbed Mn-TCNQ network, as depicted in Fig. 4. We considered a positively charged (+2) cluster with the central $Mn^{2+}$ ion carrying either five (HS) or three (IS) unpaired electrons. The simulated Mn $L_{2,3}$ NEXAFS spectra are compared with the experimental ones in Fig. 5.

The simulated spectra of the IS state do not display the complex satellite structure observed experimentally. In particular, a major discrepancy appears at the $L_2$ edge, whose experimental splitting in two equivalent components is missing in the IS state simulation. On the contrary, the simulated spectra for the HS state reproduce the following experimental observations: (i) the excitation energy (EE) separation between the $L_2$ and $L_3$ main features (10.7 eV compared with an experimental value of 11.6 eV); (ii) the change of intensity of the resonances between spectra recorded in s- and p-polarization; iii) the two main resonances at the $L_2$ edge, (iv) the satellite features observed at both the higher and lower EE side of the $L_3$ most intense line. Most importantly, although the relative intensity of the main $L_3$ line with respect to its satellite resonances shows minor discrepancies (see Fig. 6), the intensity dependence on polarization orientation of both satellites and main line are correctly reproduced, which prove the reliability of our calculations. The observed good agreement between the HS simulated and the experimental spectra consigues a strong support to the results of DFT + U calculations, which predict that the atomic and electronic structures of the Mn-TCNQ MOCN synthesized on the modified Cu(100) surface are very close to those of the unsupported counterpart.

We can thus enter into details of the nature of the multiple transitions

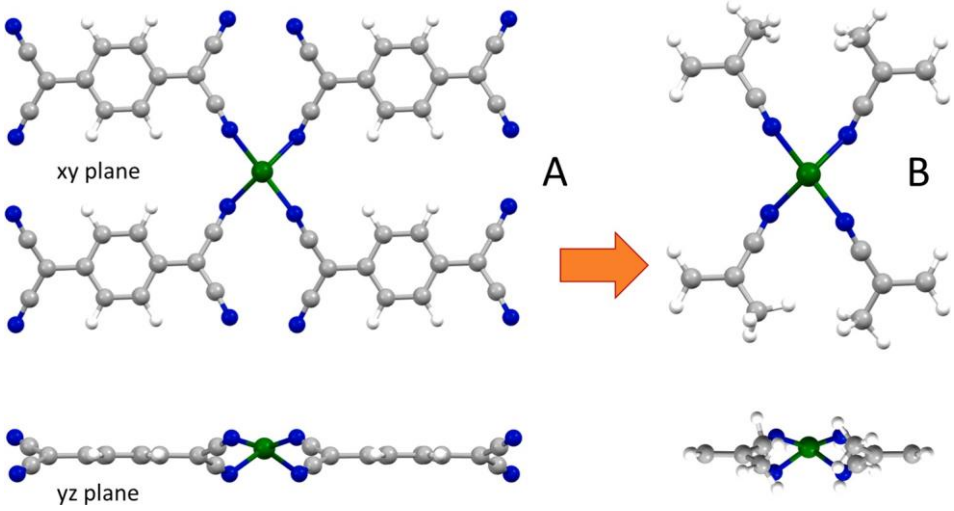


**Fig. 4.** (A) Environment of the Mn atoms in the synthetized Mn-TCNQ periodic structure. (B) Cluster model used to simulate the experimental Mn $L_{2,3}$-edges XAS resonances. Grey, white, blue and green spheres correspond to C, H, N and Mn atoms, respectively. (For interpretation of the references to colour in this figure legend, the reader is referred to the web version of this article.)

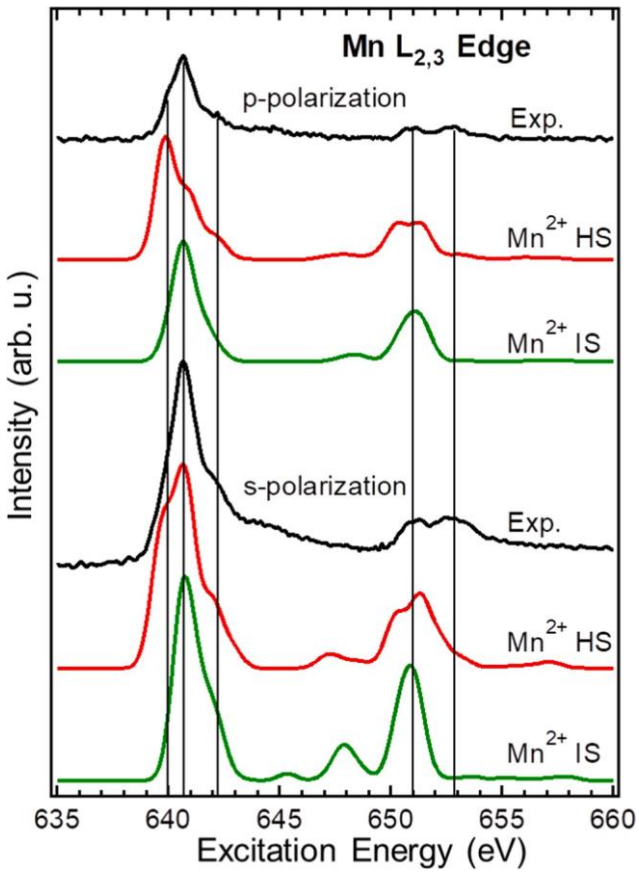


**Fig. 5.** Comparison of experimental (black) with the simulated $Mn^{2+}$ IS (green) and $Mn^{2+}$ HS (red) Mn $L_{2,3}$ NEXAFS spectra. Top and bottom panels correspond to p- and s-polarization, respectively. The simulated spectra have been shifted by 9.2 eV ($Mn^{2+}$ IS) and 9.5 eV ($Mn^{2+}$ HS) in order to align (s-polarization) the maxima of the simulated $L_3$ lines with the corresponding experimental one. A Gaussian broadening of 1 eV has been applied to all simulated spectra. The vertical lines indicate the main features of the experimental spectra, as in Fig. 3 (b). (For interpretation of the references to colour in this figure legend, the reader is referred to the web version of this article.)

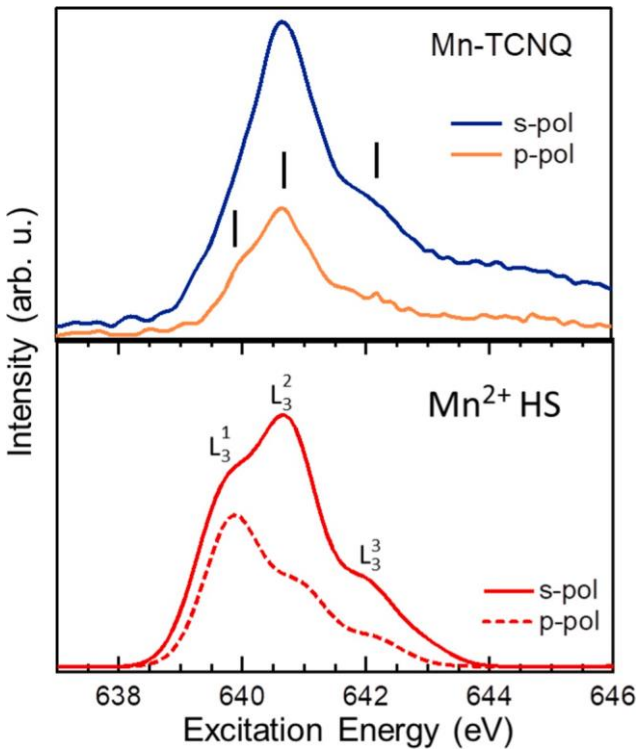


**Fig. 6.** Comparison of the measured $Mn^{2+}$ $L_3$ absorption lines (top panel) with the corresponding simulated ones obtained by assuming a HS configuration (bottom panel). See text for a detailed analysis of the main contributions to this line.

(.i.e. origin and localization). The analysis of the electronic transitions associated with electronic states generating the $L_3$-edge region indicates that, for both polarizations, only single electronic excitations are involved. From a close view of the simulated $L_3$ edge in the 638–644 eV range, we can recognize three main groups of excitations (see Fig. 6), that can be associated with the corresponding experimental NEXAFS resonances in p- and s-polarization. More specifically, the $L_3^1$ shoulder at 639.9 eV arises exclusively from states having the ground state spin multiplicity (i.e. S = 5/2, ΔS = 0) and involving Mn 2*p* transitions into four single occupied molecular orbitals (SOMOs), namely $3d_{x2-y2}$, $3d_{z2}$, $3d_{yz}$ and $3d_{xz}$. The five SOMOs as well as the most relevant virtual molecular orbitals (VMOs) are displayed in Fig. 7.

The most intense resonance $L_3^2$ at 640.7 eV includes states with ΔS = 0 (82% and 61% in s- and p-polarization, respectively) and ΔS = —1 (18% and 29% in s- and p-polarization). Similarly to the $L_3^1$ transitions, the electronic states having ΔS = 0 (S = 5/2) correspond to Mn 2*p* transitions to the SOMOs; in this case, all of them yield a contribution, even considering that the transition to the $3d_{xy}$ SOMO is only present in s-polarization. Instead, the states with ΔS = —1 (S = 3/2) are associated with Mn 2*p* transitions to π*- (VMOs) having a metal-to-ligand-charge-transfer (MLCT) character (namely LUMO, LUMO + 1 and LUMO + 2). See Fig. 7. As far as the $L_3^3$ feature (642.2 eV) is concerned, our simulations suggest to assign it to electronic states with ΔS = —1 (69% and 75% in s- and p-polarization) involving MLCT transitions that span quite a large number of ligand-based π*-symmetry VMOs (from LUMO to LUMO + 6). Minor contributions due to ΔS = 0 (S = 5/2) involve the Mn $2p \rightarrow 3d_{z2}, 3d_{xz}, 3d_{yz}$ transitions for both polarizations.

In conclusion, the overall high spin (S = 5/2) state of the $Mn^{2+}$ has to be ascribed mainly to the first two leading resonances of the $L_3$ absorption line, while the resonance at higher EE is largely contributed from transitions (charge-transfer) to ligand-base VMOs with S = 3/2 intermediate spin character. From an experimental point of view, the low energy shoulder at ~ 639.9 eV (more pronounced in p-polarization) thus represents the most clear footprint of the high spin state of Mn in the MOCN complex.

## 3. Conclusions

We have studied the detailed electronic structure of a MOCN synthetized on copper, where the central Mn ion is coordinated to four nitrile groups in a square closely-planar geometry, which mimics the tetrapyrrolic pocket of porphyrins/phthalocyanines. We have shown that the ionization and spin state of the Mn ion can be unambiguously determined by polarization dependent measurements of the Mn $L_{2,3}$ NEXAFS resonances, as simulated by the DFT/ROCIS method. The $Mn^{2+}$ ions are found in a high-spin state (S = 5/2), which is characteristic of this specific Mn-TCNQ squared complex in a free-standing, or highly decoupled, configuration [5–9], and makes this MOCN a very attractive molecular film for the integration in a layered architecture. Most importantly, the Sn alloying of the copper substrate is shown to be a promising strategy for a widespread use of Cu as a buffer layer on ferromagnetic substrates/crystals in order to integrate molecular magnets of diverse nature into layered architectures.

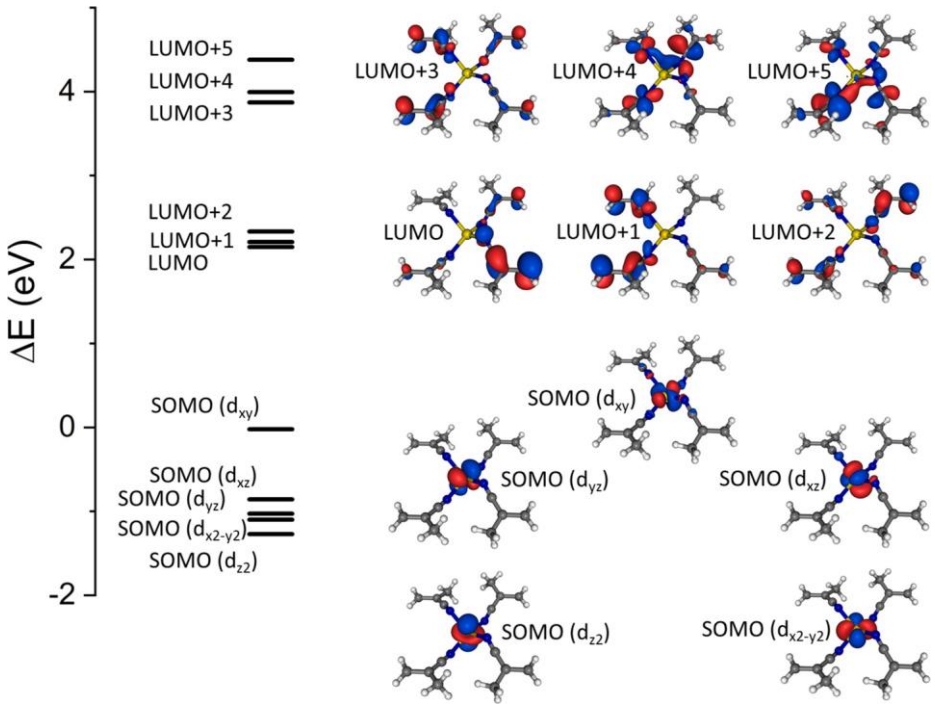


**Fig. 7.** 3D contour plots for the Singly Occupied Mn-based 3d MOs and for the six low-lying ligand-based virtual MOs for the $Mn^{2+}$ HS cluster.

## CRediT authorship contribution statement

**Silvia Carlotto:** Methodology, Investigation, Formal analysis, Writing - review & editing. **Javier D. Fuhr:** Methodology, Investigation, Formal analysis, Writing - review & editing. **Albano Cossaro:** Investigation, Formal analysis. **Alberto Verdini:** Investigation, Formal analysis. **Maurizio Casarin:** Methodology, Writing - review & editing, Supervision. **Magalí Lingenfelder:** Conceptualization, Funding acquisition, Writing - review & editing. **Julio E. Gayone:** Funding acquisition, Methodology, Investigation, Writing - review & editing. **Luca Floreano:** Conceptualization, Investigation, Writing - review & editing, Supervision. **Hugo Ascolani:** Conceptualization, Funding acquisition, Methodology, Investigation, Formal analysis, Writing - original draft, Supervision.

## Declaration of Competing Interest

The authors declare that they have no known competing financial interests or personal relationships that could have appeared to influence the work reported in this paper.

## Acknowledgements

We acknowledge financial support by the following Argentine institutions: CONICET and ANPCYT (PICT-2015–0922). We also acknowledge financial support from the ICTP-ELETTRA USERS PROGRAMME. We thank the “Centro de Simulacio´n Computacional p/ Aplicaciones Tecnolo´gicas” (CSC-CONICET) for granting the use of computational resources which allowed us to perform part of the simulations included in this work.

## Appendix A. Supplementary data

## References

[1] R. Gutzler, S. Stepanow, D. Grumelli, M. Lingenfelder, K. Kern, Mimicking enzymatic active sites on surfaces for energy conversion chemistry, Acc. Chem. Res. 48 (2015) 2132–2139, https://doi.org/10.1021/acs.accounts.5b00172.

[2] L. Dong, Z. Gao, N. Lin, Self-assembly of metal-organic coordination structures on surfaces, Prog. Surf. Sci. 91 (2016) 101–135, https://doi.org/10.1016/j.progsurf.2016.08.001.

[3] T.R. Umbach, M. Bernien, C.F. Hermanns, A. Kruger, V. Sessi, I. Fernandez-Torrente, P. Stoll, J.I. Pascual, K.J. Franke, W. Kuch, Ferromagnetic coupling of mononuclear fe centers in a self-assembled metal-organic network on au(111), Phys. Rev. Lett 109 (2012) 267207, https://doi.org/10.1103/PhysRevLett.109.267207.

[4] N. Abdurakhmanova, T.-C. Tseng, A. Langner, C. Kley, V. Sessi, S. Stepanow, K. Kern, Superexchange-mediated ferromagnetic coupling in two-dimensional ni-tcnq networks on metal surfaces, Phys. Rev. Lett. 110 (2) (2013) 027202, https://doi.org/10.1103/PhysRevLett.110.027202.

[5] M. Faraggi, N. Jiang, N. Gonzalez-Lakunza, A. Langner, S. Stepanow, K. Kern, A. Arnau, Bonding and charge transfer in metalorganic coordination networks on au(111) with strong acceptor molecules, J. Phys. Chem. C 116 (46) (2012) 24558–24565, https://doi.org/10.1021/jp306780n.

[6] L. Giovanelli, A. Savoyant, M. Abel, F. Maccherozzi, Y. Ksari, M. Koudia, R. Hayn, F. Choueikani, Otero, P. Ohresser, J.-M. Themlin, S.S. Dhesi, S. Clair, Magnetic coupling and single-ion anisotropy in surface-supported mn-based metal-organic networks, J. Phys. Chem. C 118 (2014) 11738–11744, https://doi.org/10.1021/jp502209q.

[7] M. Faraggi, V. Golovach, S. Stepanow, T.-C. Tseng, N. Abdurakhmanova, C. Kley, A. Langner, V. Sessi, K. Kern, A. Arnau, Modeling ferro- and antiferromagnetic interactions in metal-organic coordination networks, J. Phys. Chem. C 119 (46) (2015) 547–555, https://doi.org/10.1021/jp512019w.

[8] M. Blanco-Rey, A. Sarasola, C. Nistor, L. Persichetti, C. Stamm, C. Piamonteze, P. Gambardella, S. Stepanow, M. Otrokov, V. Golovach, A. Arnau, Magnetic properties of metal-organic coordination networks based on 3d transition metal atoms, Molecules 23 (2018) 964, https://doi.org/10.3390/molecules23040964.

[9] Y. Ma, Y. Dai, W. Wei, L. Yu, B. Huang, Novel two-dimensional tetragonal monolayer: Metal-tcnq networks, J. Phys. Chem. A 117 (2013) 5171–5177, https://doi.org/10.1021/jp402637f.

[10] T.-C. Tseng, C. Lin, X. Shi, S. Tait, X. Liu, U. Starke, N. Lin, R. Zhang, C. Minot, M.A. V. Hove, J. Cerda´, K. Kern, Two-dimensional metal-organic coordination networks of mn-7,7,8,8-tetracyanoquinodimethane assembled on cu(100): Structural, electronic, and magnetic properties, Phys. Rev. B 80 (2009) 155458, https://doi.org/10.1103/PhysRevB.80.155458.

[11] A. Cebollada, R. Miranda, C. Schneider, P. Schuster, J. Kirschner, Experimental evidence of an oscillatory magnetic coupling in co/ cu/ co epitaxial layers, J. Magn. Magn. Mater. 102 (1) (1991) 25–29, https://doi.org/10.1016/0304-8853(91)90259-D.

[12] Y. Kawawake, H. Sakakima, Magnetoresistance in epitaxial [nife/cu/co(/cu)] films, J. Magn. Magn. Mater. 149 (3) (1995) L255–L259, https://doi.org/10.1016/0304-8853(95)00289-8.

[13] Y.Z. Wu, A.K. Schmid, M.S. Altman, X.F. Jin, Z.Q. Qiu, Spin-dependent fabry-pe´rot interference from a cu thin film grown on fcc co(001), Phys. Rev. Lett. 94 (2005) 027201, https://doi.org/10.1103/PhysRevLett.94.027201.
[14] G. Polzonetti, V. Di Castro, C. Furlani, The growth mode of copper and iron for the cu/fe and fe/cu interfaces, Surf. Interface Anal. 22 (1994) 211–213, https://doi.org/10.1002/sia.740220147.
[15] G. Gubbiotti, L. Albini, S. Tacchi, G. Carlotti, R. Gunnella, M. De Crescenzi, Structural and magnetic properties of epitaxial cu/fe/cu/si(111) ultrathin films, Phys. Rev. B 60 (1999) 17150–17161, https://doi.org/10.1103/PhysRevB.60.17150.
[16] B. Müller, L. Nedelmann, B. Fischer, H. Brune, K. Kern, Initial stages of cu epitaxy on ni(100): Postnucleation and a well-defined transition in critical island size, Phys. Rev. B 54 (1996) 17858–17865, https://doi.org/10.1103/PhysRevB.54.17858.
[17] P.F.A. Alkemade, H. Fortuin, R. Balkenende, F.H.P.M. Habraken, W.F. van der Weg, The epitaxial growth of nickel on cu(100) studied by ion channeling, in: J. F. van der Veen, M.A. Van Hove (Eds.), The Structure of Surfaces II, Springer, Berlin Heidelberg, Berlin, Heidelberg, 1988, pp. 443–449.
[18] G. Zamborlini, M. Jugovac, A. Cossaro, A. Verdini, L. Floreano, D. Lüftner, P. Puschnig, V. Feyer, C.M. Schneider, On-surface nickel porphyrin mimics the reactive center of an enzyme cofactor, Chem. Commun. 54 (2018) 13423–13426, https://doi.org/10.1039/C8CC06739B.
[19] C.M. Doyle, J.P. Cunniffe, S.A. Krasnikov, A.B. Preobrajenski, Z. Li, N.N. Sergeeva, M.O. Senged, A.A. Cafolla, Ni-cu ion exchange observed for ni(ii)-porphyrins on cu (111), Chem. Comm. 50 (2014) 3447–3449, https://doi.org/10.1039/c3cc48913b.
[20] M. Franke, F. Marchini, N. Jux, H.-P. Steinrück, O. Lytken, F.J. Williams, Zinc porphyrin metal-center exchange at the solid-liquid interface, Chem. A Eur. J. 22 (25) (2016) 8520–8524, https://doi.org/10.1002/chem.201600634.
[21] K. Shen, B. Narsu, G. Ji, H. Sun, J. Hu, Z. Liang, X. Gao, H. Li, Z. Li, B. Song, Z. Jiang, H. Huang, J.W. Wells, F. Song, On-surface manipulation of atom substitution between cobalt phthalocyanine and the cu(111) substrate, RSC Adv. 7 (2017) 13827–13835, https://doi.org/10.1039/C7RA00636E.
[22] A. Rieger, S. Schnidrig, B. Probst, K.-H. Ernst, C. Wa¨ckerlin, Ranking the stability of transition-metal complexes by on-surface atom exchange, J. Phys. Chem. Lett. 8 (24) (2017) 6193–6198, https://doi.org/10.1021/acs.jpclett.7b02834.
[23] A. Carrera, L. Cristina, S. Bengi'o, A. Cossaro, A. Verdini, L. Floreano, J. Fuhr, J. Gayone, H. Ascolani, Controlling carboxyl deprotonation on cu(001) by surface sn alloying, J. Phys. Chem C 117 (2013) 17058–17065, https://doi.org/10.1021/jp404983n.
[24] J. Fuhr, M. van der Meijden, L. Cristina, L. Rodríguez, R. Kellogg, J. Gayone, H. Ascolani, M. Lingenfelder, Chiral expression of adsorbed (mp) 5-amino[6]helicenes: from random structures to dense racemic crystals by surface alloying, Chem. Commun. 53 (2017) 130–133, https://doi.org/10.1039/C6CC06785A.
[25] B.Q. Argan˜araz, L. Cristina, L. Rodríguez, A. Cossaro, A. Verdini, L. Floreano, J. Fuhr, J. Gayone, H. Ascolani, Ubiquitous deprotonation of terephthalic acid in the self-assembled phases on cu(100), Phys. Chem. Chem. Phys. 20 (2018) 4319, https://doi.org/10.1039/C7CP06612K.
[26] L.M. Rodríguez, a J.D. Fuhr, P. Machaín, H. Ascolani, M. Lingenfelder, J.E. Gayone, Building two-dimensional metal-organic networks with tin, Chem. Commun. 55 (2019) 345–348, https://doi.org/10.1039/C8CC08280D.
[27] P. Machaín, J.D. Fuhr, S. Schneider, S. Carlotto, M. Casarin, A. Cossaro, A. Verdini, L. Floreano, M. Lingenfelder, J.E. Gayone, H. Ascolani, Mn-cu transmetalation as a strategy for the assembly of decoupled metal-organic networks on sn/cu(001) surface alloys, J. Phys. Chem. C 124 (35) (2020) 18993–19002, https://doi.org/10.1021/acs.jpcc.0c03395.
[28] E.I. Solomon, B. Hedman, K.O. Hodgson, A. Dey, R.K. Szilagyi, Ligand k-edge x-ray absorption spectroscopy: covalency of ligand-metal bonds, Coord. Chem. Rev. 249 (1) (2005) 97–129, https://doi.org/10.1016/j.ccr.2004.03.020, synchrotron Radiation in Inorganic and Bioinorganic Chemistry.
[29] F. de Groot, Multiplet effects in x-ray spectroscopy, Coord. Chem. Rev. 249 (1) (2005) 31–63, https://doi.org/10.1016/j.ccr.2004.03.018, synchrotron Radiation in Inorganic and Bioinorganic Chemistry.
[30] G. Mangione, S. Carlotto, M. Sambi, G. Ligorio, M. Timpel, A. Vittadini, M.V. Nardi, M. Casarin, Electronic structures of cutpp and cutpp(f) complexes. a combined experimental and theoretical study i, Phys. Chem. Chem. Phys. 18 (2016) 18727–18738, https://doi.org/10.1039/C6CP01423B.
[31] S. Carlotto, M. Sambi, M. Rancan, M. Casarin, Theoretical investigation of the electronic properties of three vanadium phthalocyaninato (pc) based complexes: Pcv, pcvo, and pcvi, Inorg. Chem. 57 (4) (2018) 1859–1869, https://doi.org/10.1021/acs.inorgchem.7b02788.
[32] L. Floreano, G. Naletto, D. Cvetko, R. Gotter, M. Malvezzi, L. Marassi, A. Morgante, A. Santaniello, A. Verdini, F. Tommasini, G. Tondello, Performance of the grating-crystal monochromator of the aloisa beamline at the elettra synchrotron, Rev. Sci. Instrum. 70 (10) (1999) 3855–3864, https://doi.org/10.1063/1.1150001.
[33] J. Fuhr, L. Robino, L.M. Rodríguez, A. Verdini, L. Floreano, H. Ascolani, J. Gayone, 2d cu-tcnq metal-organic networks induced by surface alloying, J. Phys. Chem. C 124 (1) (2020) 416–424, https://doi.org/10.1021/acs.jpcc.9b08430.
[34] L. Floreano, A. Cossaro, R. Gotter, A. Verdini, G. Bavdek, F. Evangelista, A. Ruocco, A. Morgante, D. Cvetko, Periodic arrays of cu-phthalocyanine chains on au(110), J. Phys. Chem. C 112 (29) (2008) 10794–10802, https://doi.org/10.1021/jp711140e.
[35] P. Giannozzi, S. Baroni, N. Bonini, M. Calandra, R. Car, C. Cavazzoni, D. Ceresoli, G.L. Chiarotti, M. Cococcioni, I. Dabo, J. Phys.: Condens. Matter 21 (2009) 395502.
[36] F. Neese, The orca program system, WIREs Comput. Mol. Sci. 2 (1) (2012) 73–78, https://doi.org/10.1002/wcms.81.
[37] Y. Zhao, D.G. Truhlar, The m06 suite of density functionals for main group thermochemistry, thermochemical kinetics, noncovalent interactions, excited states, and transition elements: two new functionals and systematic testing of four m06-class functionals and 12 other functionals, Theoret. Chem. Acc. 120 (1) (2008) 215–241, https://doi.org/10.1007/s00214-007-0310-x.
[38] F. Weigend, Accurate coulomb-fitting basis sets for h to rn, Phys. Chem. Chem. Phys. 8 (2006) 1057–1065, https://doi.org/10.1039/B515623H.
[39] S. Carlotto, M. Sambi, A. Vittadini, M. Casarin, Mn(acac)2 and mn(acac)3 complexes, a theoretical modeling of their l2,3-edges x-ray absorption spectra, Polyhedron 135 (2017) 216–223, https://doi.org/10.1016/j.poly.2017.07.007.
[40] S. Carlotto, L. Floreano, A. Cossaro, M. Dominguez, M. Rancan, M. Sambi, M. Casarin, The electronic properties of three popular high spin complexes [tm (acac)3, tm =cr, mn, and fe] revisited: an experimental and theoretical study, Phys. Chem. Chem. Phys. 19 (2017) 24840–24854, https://doi.org/10.1039/C7CP04461E.
[41] M. Roemelt, D. Maganas, S. DeBeer, F. Neese, A combined dft and restricted open-shell configuration interaction method including spin-orbit coupling: Application to transition metal l-edge x-ray absorption spectroscopy, J. Chem. Phys. 138 (20) (2013) 204101, https://doi.org/10.1063/1.4804607.
[42] D. Maganas, M. Roemelt, T. Weyhermüller, R. Blume, M. Ha¨vecker, A. Knop-Gericke, S. DeBeer, R. Schlo¨gl, F. Neese, L-edge x-ray absorption study of mononuclear vanadium complexes and spectral predictions using a restricted open shell configuration interaction ansatz, Phys. Chem. Chem. Phys. 16 (2014) 264–276, https://doi.org/10.1039/C3CP52711E.
[43] D.A. Pantazis, X.-Y. Chen, C.R. Landis, F. Neese, All-electron scalar relativistic basis sets for third-row transition metal atoms, J. Chem. Theory Comput. 4 (6) (2008) 908–919, https://doi.org/10.1021/ct800047t, pMID: 26621232.
[44] C. Van Alsenoy, Ab initio calculations on large molecules: The multiplicative integral approximation, J. Comput. Chem. 9 (6) (1988) 620–626, https://doi.org/10.1002/jcc.540090607.
[45] D. Coster, R.D.L. Kronig, New type of auger effect and its influence on the x-ray spectrum, Physica 2 (1) (1935) 13–24, https://doi.org/10.1016/S0031-8914(35)90060-X.
[46] M. B¨assler, R. Fink, C. Buchberger, P. V¨aterlein, M. Jung, E. Umbach, Near edge x-ray absorption fine structure resonances of quinoide molecules, Langmuir 16 (2000) 6674–6681, https://doi.org/10.1021/la0002536.
[47] J. Fraxedas, Y.J. Lee, I. Jim´enez, R. Gago, R.M. Nieminen, P. Ordejo´n, E. Canadell, Characterization of the unoccupied and partially occupied states of ttf-tcnq by xanes and first-principles calculations, Phys. Rev. B 68 (2003) 195115, https://doi.org/10.1103/PhysRevB.68.195115.
[48] R.K. Hocking, E.I. Solomon, Ligand field and molecular orbital theories of transition metal X-ray absorption edge transitions., in: D. Mingos, P. Day, J. Dahl, Eds. Molecular Electronic Structures of Transition Metal Complexes I. Structure and Bonding 142 (2011) 155–184. doi:10.1007/430_2011_60.
[49] S. Carlotto, M. Sambi, F. Sedona, A. Vittadini, M. Casarin, A theoretical study of the occupied and unoccupied electronic structure of high- and intermediate-spin transition metal phthalocyaninato (pc) complexes: Vpc, crpc, mnpc, and fepc, Nanomaterials 11 (2021) 54, https://doi.org/10.3390/nano11010054.
[50] M.E. Ali, B. Sanyal, P.M. Oppeneer, Tuning the magnetic interaction between manganese porphyrins and ferromagnetic co substrate through dedicated control of the adsorption, J. Phys. Chem. C 113 (2009) 14381–14383, https://doi.org/10.1021/jp902644q.
[51] S. Stepanow, A. Rizzini, C. Krull, J. Kavich, J. Cezar, F. Yakhou-Harris, P. Sheverdyaeva, P. Moras, C. Carbone, G. Ceballos, A. Mugarza, P. Gambardella, Spin tuning of electron-doped metal-phthalocyanine layers, J. Am. Chem Soc 136 (2014) 5451–5459, https://doi.org/10.1021/ja501204q.
[52] M. Mabrouk, R. Hayn, Magnetic moment formation in metal-organic monolayers, Phys. Rev. B 92 (2015) 184424, https://doi.org/10.1103/PhysRevB.92.184424.